Journal of Applied Electrochemistry **31**: 1243–1249, 2001.

Electrical conduction behaviour of Ba^{2+} and Mg^{2+} doped $LaGaO_3$ perovskite oxide

K.T. LEE[1], S. KIM[2], G.D. KIM[3] and H.L. LEE[1]*
[1]*Department of Ceramic Engineering, Yonsei University, Seoul 120-749, Korea*
[2]*Engineering Research Institute, Yonsei University, Seoul 120-749, Korea*
[3]*Korea Institute of Science & Technology, Seoul 136-791, Korea*
*(*author for correspondence, fax: +82 2 365 5882, e-mail: htm@yonsei.ac.kr)*

Received 10 October 2000; accepted in revised form 26 June 2001

Key words: activation energy, association, $LaGaO_3$, oxygen ion conductivity, oxygen vacancy

Abstract

The electrical properties of Ba^{2+} and Mg^{2+} doped $LaGaO_3$ perovskite oxide were investigated. Doping with either Ba^{2+} or Mg^{2+} enhanced oxygen ion conductivity. The grain boundary resistance decreased with increasing Mg^{2+} concentration due to a reduced second phase concentration. The activation energy for oxygen ion conduction is much higher in a low-temperature region than in a high-temperature region.

1. Introduction

Oxygen ion conductors have attracted much attention as functional materials for technical applications (e.g., solid oxide fuel cells, oxygen sensors). It is well known that oxides with fluorite structure such as Y_2O_3-stabilized ZrO_2 (YSZ), exhibit good oxygen ion conductivity [1]. However, the high operating temperature (above 1000 °C) for YSZ reduces the reliability and restricts the choice of materials for fuel cell stacking. Therefore, the development of an oxide with high oxygen ion conductivity at reduced temperature (below 1000 °C) is of great importance. A doped ceria electrolyte shows high oxygen conductivity at reduced temperatures. However, a ceria-based electrolyte exhibits electronic conduction in a reducing atmosphere, which decreases the open circuit voltage from the theoretical value [2]. Consequently, there is a need for new electrolyte materials with high oxygen ion conductivity over a wide oxygen partial pressure range, as well as at reduced temperatures.

It has been reported that the doped $LaGaO_3$ perovskite oxides show high oxygen ion conductivity and also allow a wider range in the choice of electrode materials than fluorite structure electrolytes [3–5]. In particular, $LaGaO_3$ doped with Sr^{2+} and Mg^{2+} was recently reported to exhibit superior oxygen ion conductivity to that of YSZ [6–8]. However, most recent investigations have been focused on $La_{1-x}Sr_xGa_{1-y}Mg_yO_{3-\delta}$ system (LSGM).

Stevenson et al. reported that the oxygen ion conductivity of $La_{0.90}Ba_{0.10}Ga_{0.80}Mg_{0.20}O_{3-\delta}$ was similar to that of $La_{0.90}Sr_{0.10}Ga_{0.80}Mg_{0.20}O_{3-\delta}$ and the thermal expansion coefficient value of $La_{0.90}Ba_{0.10}Ga_{0.80}Mg_{0.20}O_{3-\delta}$ was higher than that of $La_{0.90}Sr_{0.10}Ga_{0.80}Mg_{0.20}O_{3-\delta}$ [9]. However, the $La_{1-x}Ba_xGa_{1-y}Mg_yO_{3-\delta}$ system (LBGM) has not been further investigated. In this work we have studied the electrical properties of the $La_{1-x}Ba_xGa_{1-y}Mg_yO_{3-\delta}$ system with variation with Ba^{2+} and Mg^{2+} concentration.

2. Experimental procedure

The LBGM samples were made by solid-state reaction. La_2O_3 (>99.9%), Ga_2O_3 (>99.9%), $BaCO_3$ (>99.9%), and MgO (>99.9%) were used as starting materials. Before weighing, La_2O_3 and MgO were fired at 1000 °C for 1 h in order to remove hydroxides and carbonates. The required amounts of batch powders were thoroughly mixed in an agate mortar. Pellets were made from the mixed powders and then fired at 1100 °C for 5 h in air. After regrinding, the mixture was pressed isostatically into bar-type and disc-type specimens. The specimens sintered at 1500 °C for 10 h in air and were examined by powder X-ray diffraction (Rigaku Rint 2700). The microstructures of the sintered specimens were observed using SEM (Hitachi S-2700). The electrical conductivity of the specimens was measured as a function of temperature (400–1200 °C) by the conventional dc four-probe method. Two-probe impedance spectroscopy was used to separate the grain-boundary contribution from the overall conductivity with an impedance analyzer (Solatron 1260A). The frequency range used in all the experiments was 0.1 Hz–3.2 MHz and the amplitude of the input sine-wave signal was 50 mV.

3. Results and discussion

3.1. *Powder X-ray diffraction*

Figure 1 shows the X-ray diffraction patterns of $La_{0.95}Ba_{0.05}Ga_{1-y}Mg_yO_{3-\delta}$ (y = 0, 0.05, 0.10, 0.15, 0.20, 0.25, 0.30). A single phase was observed for all compositions of the $La_{0.95}Ba_{0.05}Ga_{1-y}Mg_yO_{3-\delta}$ system except for $La_{0.90}Ba_{0.05}GaO_{3-\delta}$ (LBGM-0500) and $La_{0.95}Ba_{0.05}Ga_{0.95}Mg_{0.05}O_{3-\delta}$ (LBGM-0505). This means that the solubility limit of Ba^{2+} on the La^{3+} sites in $LaGaO_3$ system is below 5 at % at 1500 °C sintering condition. The secondary phase of $La_{0.95}Ba_{0.05}Ga_{1-y}Mg_yO_{3-\delta}$ system is recognized as $BaLaGa_3O_7$ (JCPDS 24-0107). The result that no diffraction peak of secondary phases was observed at compositions which contained more than 10 at % Mg^{2+} dopants implies that the solubility limit of Ba^{2+} on the La^{3+} sites increases by substituting Mg^{2+} on Ga^{3+} sites in $LaGaO_3$ system. This is similar to the result from the X-ray diffraction patterns of $La_{0.90}Ba_{0.10}Ga_{1-y}Mg_yO_{3-\delta}$ (y = 0, 0.05, 0.10, 0.15, 0.20, 0.25, 0.30) in Figure 2. The solubility limit of Ba^{2+} on the La^{3+} sites increases up to 10 at % as the substitution amount of Mg^{2+} on Ga^{3+} sites increases to over 20 at %. In addition to $BaLaGa_3O_7$ another unknown peak was detected at compositions which contained less than 20 at % Mg^{2+} dopants. This unknown secondary phase is thought to be $BaLaGaO_4$ since the peak shows a similar pattern to $SrLaGaO_4$ (JCPDS 24-1208). Huang et al. also reported that $SrLaGa_3O_7$ and $SrLaGaO_4$ were formed as secondary phases in the $La_{1-x}Sr_xGa_{1-y}Mg_yO_{3-\delta}$ system [10]. However, further studies may be required since there has been no investigation on the $BaLaGaO_4$ phase.

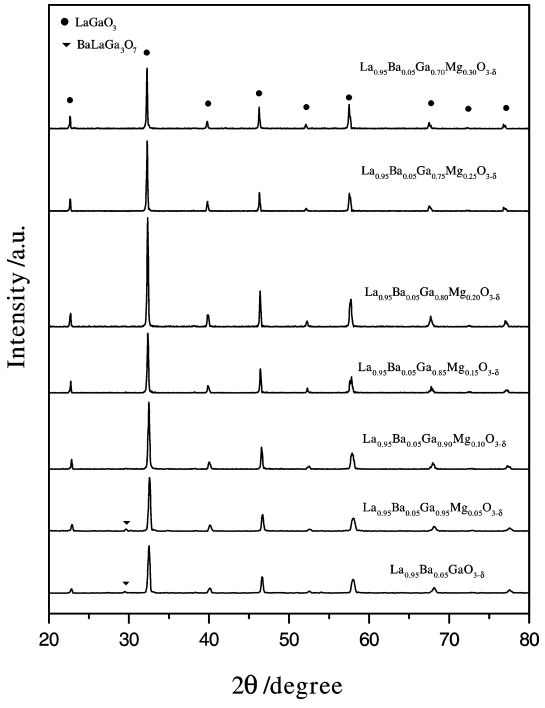

Fig. 1. X-ray diffraction patterns of $La_{0.95}Ba_{0.05}Ga_{1-y}Mg_yO_{3-\delta}$ for y values; y = 0, 0.05, 0.10, 0.15, 0.20, 0.25, 0.30 sintered at 1500 °C for 10 h.

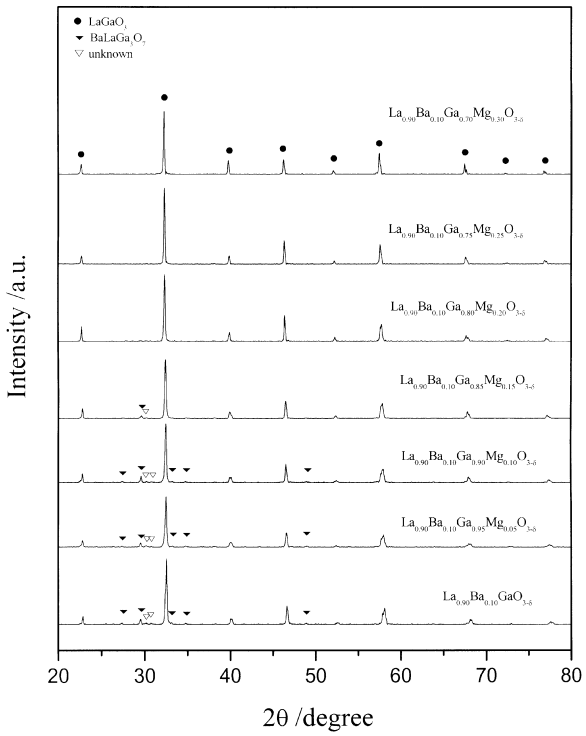

Fig. 2. X-ray diffraction patterns of $La_{0.90}Ba_{0.10}Ga_{1-y}Mg_yO_{3-\delta}$ for y values; y = 0, 0.05, 0.10, 0.15, 0.20, 0.25, 0.30 sintered at 1500 °C for 10 h.

3.2. *Oxygen ion conductivity*

The electrical conductivity of the specimens was measured in a tube-type furnace to observe the effect of the atmosphere on the electrical conductivity by the conventional d.c. four-probe method.

The ionic conductivity of solid electrolytes, σ, is represented by four terms (carrier concentration, C, carrier charge, Ze, where Z is the valence and e is the electronic charge, and carrier mobility μ).

$$\sigma = CZe\mu \tag{1}$$

The carrier mobility is given by the Nernst–Einstein relationship [11] between mobility and diffusion coefficent, D:

$$\mu = \frac{ZeD}{kT} \tag{2}$$

where k is the Boltzmann constant and T the absolute temperature. The diffusion coefficient $D = D_0 \exp(-\Delta G/kT)$ contains the motional free energy $\Delta G = \Delta H - T\Delta S$ for a jump to a vacant site. Combining Equation 1 with Equation 2 gives

$$\sigma T = A \exp\left(-\frac{E_a}{kT}\right) \tag{3}$$

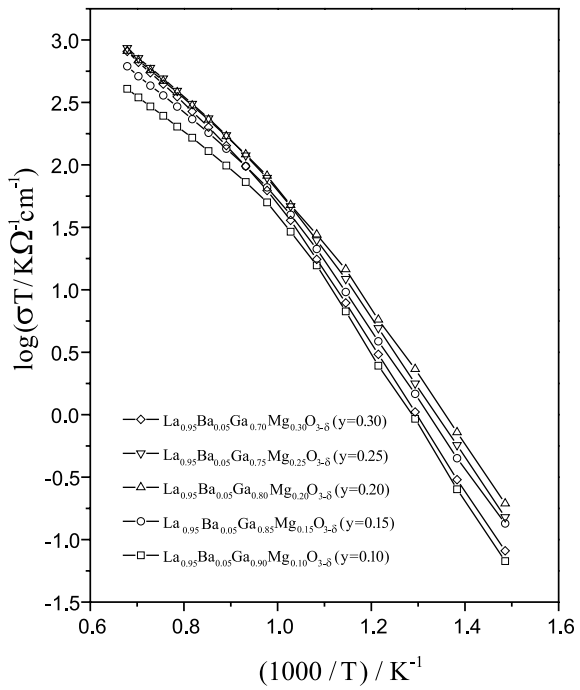

Fig. 3. Arrhenius plots of $La_{0.95}Ba_{0.05}Ga_{1-y}Mg_yO_{3-\delta}$ for y values; y = 0.10, 0.15, 0.20, 0.25, 0.30 in N_2.

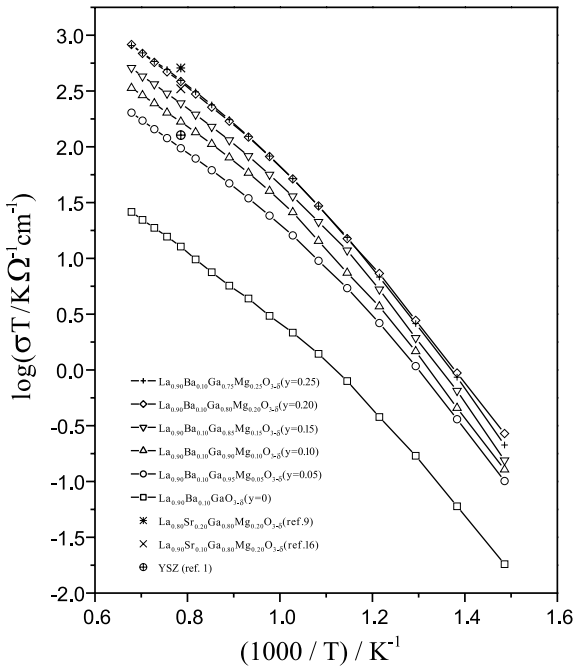

Fig. 4. Arrhenius plots of $La_{0.90}Ba_{0.10}Ga_{1-y}Mg_yO_{3-\delta}$ for y values; y = 0, 0.05, 0.10, 0.15, 0.20 0.25 in N_2.

where

$$A = \frac{CZ^2a_0^2v}{k}\exp\left(\frac{\Delta S}{k}\right) \tag{4}$$

In this equation, a_0 is the jump distance and v is Debye frequency.

The oxygen ion conductivity values of $La_{0.95}Ba_{0.05}Ga_{1-y}Mg_yO_{3-\delta}$ (y = 0.10, 0.15, 0.20, 0.25, 0.30) and $La_{0.90}Ba_{0.10}Ga_{1-y}Mg_yO_{3-\delta}$ (y = 0, 0.05, 0.10, 0.15, 0.20, 0.25) are plotted in Figures 3 and 4, respectively, according to Arrhenius (Equation 3). In the LBGM system, doping with aliovalent cations such as Ba^{2+} and Mg^{2+} results in the formation of oxygen vacancies which are the channel of oxygen ion hopping according to

$$BaO \rightarrow Ba'_{La} + O_O + \frac{1}{2}V_{\ddot{O}} \tag{5}$$

and

$$MgO \rightarrow Mg'_{Ga} + O_O + \frac{1}{2}V_{\ddot{O}} \tag{6}$$

Thus it is thought that the increase in oxygen vacancy concentration due to the substitutions of cations with lower valence makes a contribution to the increase in oxygen ion conductivity. This is also supported by the fact that there is wide difference in oxygen ion conductivities between $La_{0.90}Ba_{0.10}Ga_{0.95}Mg_{0.05}O_{3-\delta}$ (LBGM-1005) and $La_{0.90}Ba_{0.10}GaO_{3-\delta}$ (LBGM-1000) doped no Mg^{2+} in Figure 4.

The a.c. impedance spectra of $La_{0.90}Ba_{0.10}Ga_{1-y}Mg_yO_{3-\delta}$ (y = 0, 0.10, 0.20) measured at 300 °C in N_2 are shown in Figure 5. The a.c. impedance data can be resolved into three distinct arcs: a bulk arc at high frequencies (associated typical capacitance value around 1 pF), a grain boundary arc (associated typical capacitance value around 1 nF), and an electrode arc at low frequencies.

The grain boundary resistance (R_{gb}) decreased with increasing Mg^{2+} concentration. In other words the density of grain boundary decreases with increasing Mg^{2+} concentration. The composition $La_{0.90}Ba_{0.10}Ga_{0.80}Mg_{0.20}O_{3-\delta}$ (LBGM-1020) was single phase, while second phases were detected at the composition $La_{0.90}Ba_{0.10}GaO_{3-\delta}$ (LBGM-1000) and the composition $La_{0.90}Ba_{0.10}Ga_{0.90}Mg_{0.10}O_{3-\delta}$ (LBGM-1010) as shown in Figure 2. The density of grain boundary increases since the second phase such as $BaLaGa_3O_7$ formed at grain boundary hinders the grain growth. This result is consistent with the SEM microstructures in Figure 6. With increasing Mg^{2+} concentration, the grains grow bigger from 3–4 μm to about 25 μm because of reduced second phase concentration, according to the increase in solubility limit of Ba^{2+} for La^{3+} sites.

Meanwhile, the oxygen ion conductivity values of the LBGM system were slightly lower than that of $La_{0.80}Sr_{0.20}Ga_{0.80}Mg_{0.20}O_{3-\delta}$ (LSGM-2020) as shown in Figure 4. This is because the maximum solubility limit of Sr^{2+} for La^{3+} sites in $La_{1-x}Sr_xGa_{1-y}Mg_yO_{3-\delta}$ system is x = 0.20, while that of Ba^{2+} for La^{3+} site in $La_{1-x}Ba_xGa_{1-y}Mg_yO_{3-\delta}$ system is x = 0.10. However, the oxygen ion conductivity values of the LBGM system are still higher than that of YSZ. Especially, the oxygen conductivity value of $La_{0.90}Ba_{0.10}Ga_{0.80}Mg_{0.20}O_{3-\delta}$ (LBGM-1020) was 0.114 $\Omega^{-1}\,cm^{-1}$ at 800 °C, which is comparable to that of YSZ at 1000 °C. Consequently, the LBGM system is promising material as solid electrolyte for reduced-temperature ceramic fuel cells.

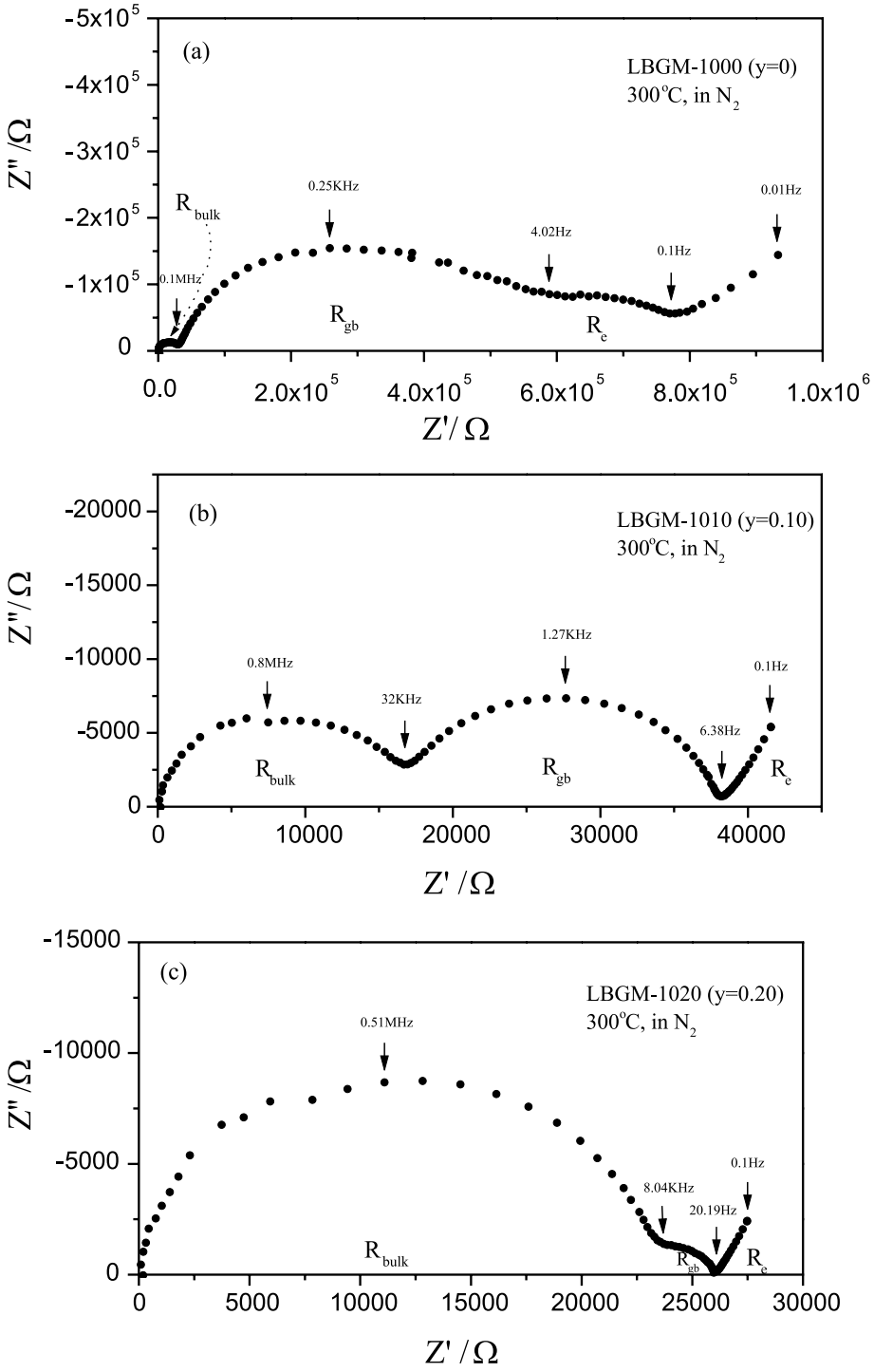

Fig. 5. AC impedance spectra of $La_{0.90}Ba_{0.10}Ga_{1-y}Mg_yO_{3-\delta}$ with Pt electrode at 300 °C in N_2: (a) $y = 0$ (b) $y = 0.10$ (c) $y = 0.20$.

Figure 7 shows the effects of Ba^{2+} doping in $La_{1-x}Ba_xGa_{0.80}Mg_{0.20}O_{3-\delta}$ ($x = 0$, 0.05, 0.10, 0.15). The oxygen ion conductivity increased with increasing Ba^{2+} concentration and then decreased at $La_{0.85}Ba_{0.15}Ga_{0.80}Mg_{0.20}O_{3-\delta}$ (LBGM-1520). This probably results from the formation of second phases, which hinder oxygen ion conduction.

Figure 8 shows the electrical conductivity values of the compositions in which no second phases were detected. Although the concentration of oxygen vacancies originating from Ba^{2+} and Mg^{2+} doping was much higher, the oxygen ion conductivities of $La_{0.85}Ba_{0.15}Ga_{0.75}Mg_{0.25}O_{3-\delta}$ (LBGM-1525) and $La_{0.90}Ba_{0.10}Ga_{0.70}Mg_{0.30}O_{3-\delta}$ (LBGM-1030) were lower than that of $La_{0.90}Ba_{0.10}Ga_{0.80}Mg_{0.20}O_{3-\delta}$ (LBGM-1020). This result might be caused by association between dopant cations and oxygen vacancies, oxygen vacancies ordering, or structural distortion due to excessive formation of oxygen vacancies.

This is also explained by the same reason that the oxygen ion conductivity of $La_{0.95}Ba_{0.05}Ga_{0.70}Mg_{0.30}O_{3-\delta}$ (LBGM-0530) is lower than that of $La_{0.95}$-

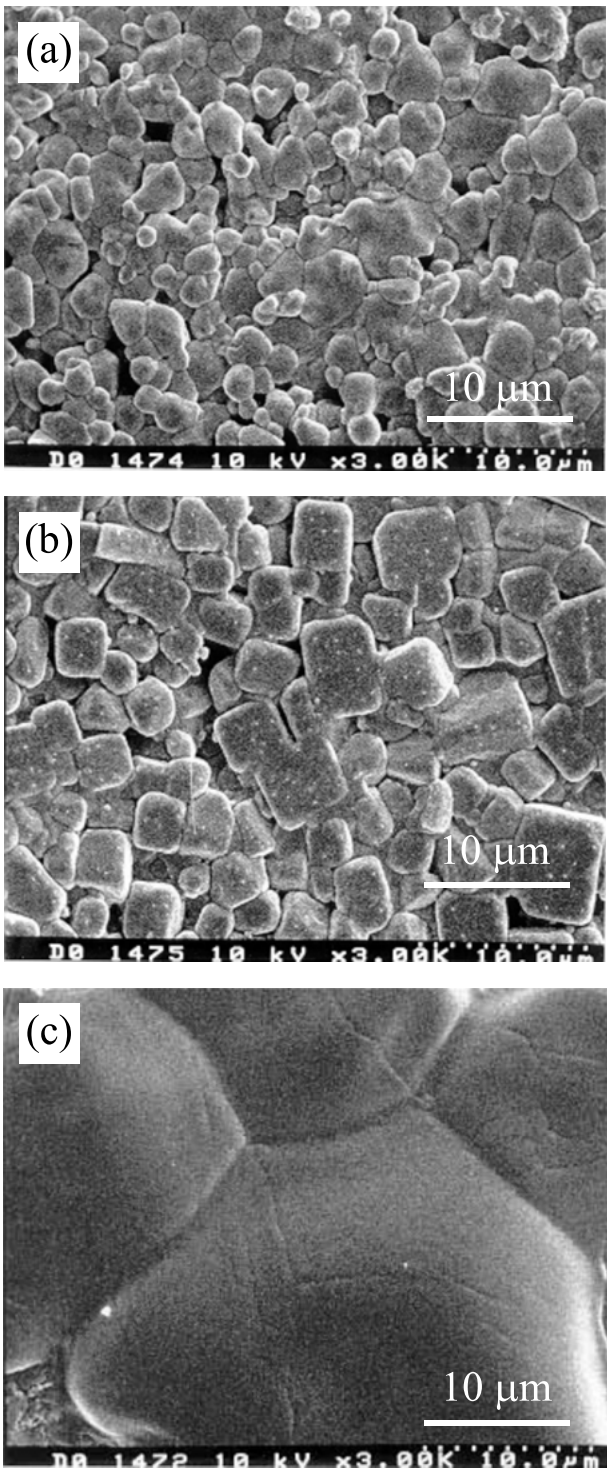

Fig. 6. SEM microstructures of $La_{0.90}Ba_{0.10}Ga_{1-y}Mg_yO_{3-\delta}$ after thermal etching at 1350 °C for 1 h: (a) $y = 0$ (b) $y = 0.10$ (c) $y = 0.20$.

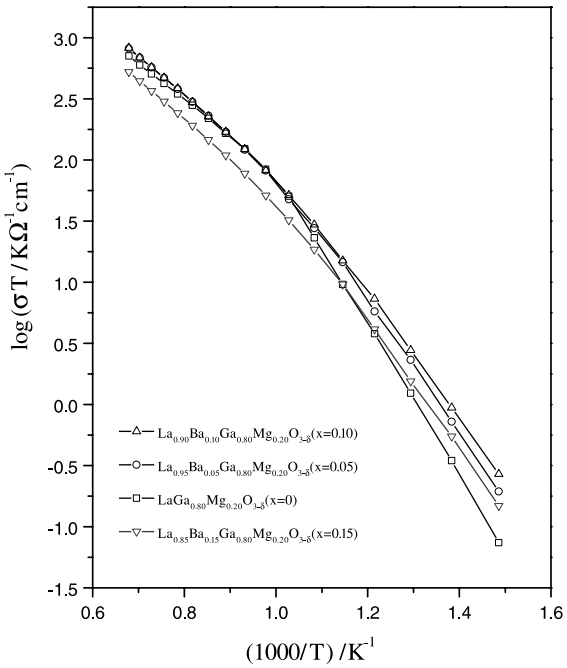

Fig. 7. Arrhenius plots of $La_{1-x}Ba_xGa_{0.80}Mg_{0.20}O_{3-\delta}$ for x values; $x = 0$, 0.05, 0.10, 0.15 in N_2.

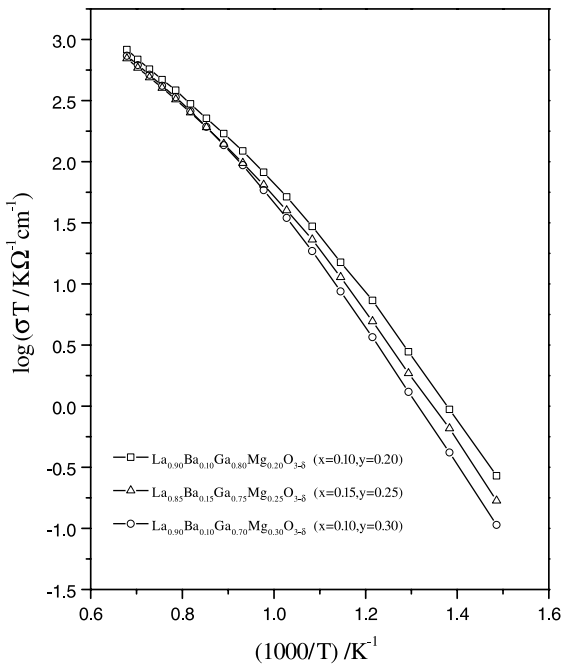

Fig. 8. Arrhenius plots of $La_{1-x}Ba_xGa_{1-y}Mg_yO_{3-\delta}$ in N_2.

$Ba_{0.05}Ga_{0.75}Mg_{0.25}O_{3-\delta}$ (LBGM-0525), and the oxygen ion conductivities of $La_{0.90}Ba_{0.10}Ga_{0.75}Mg_{0.25}O_{3-\delta}$ (LBGM-1025) and $La_{0.90}Ba_{0.10}Ga_{0.70}Mg_{0.30}O_{3-\delta}$ (LBGM-1030) are lower than that of $La_{0.90}Ba_{0.10}Ga_{0.80}Mg_{0.20}O_{3-\delta}$ (LBGM-1020) in Figures 3 and 4, respectively. This means that there might be a critical point of the amount of oxygen vacancies showing maximum oxygen ion conductivity, and the optimum amount of oxygen vacancies showing the highest oxygen ion conductivity in single phase LBGM system is about 15 at %.

Figure 9 shows the electrical conductivity of $La_{0.90}Ba_{0.10}Ga_{0.80}Mg_{0.20}O_{3-\delta}$ (LBGM-1020) as a function of oxygen partial pressure. The electrical conductivity was almost independent of the oxygen partial pressure. This suggests that this Ba^{2+} and Mg^{2+} doped $LaGaO_3$ perovskite oxide is almost a pure oxygen ion conductor over a wide range of oxygen partial pressure.

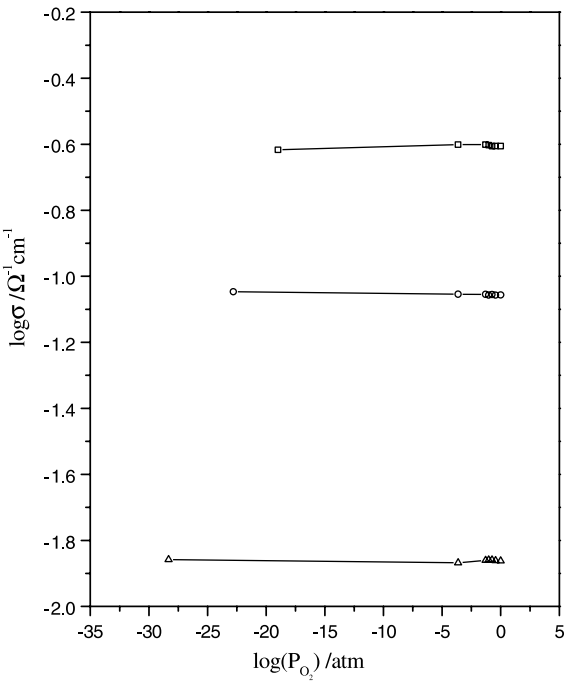

Fig. 9. Electrical conductivity of $La_{0.90}Ba_{0.10}Ga_{0.80}Mg_{0.20}O_{3-\delta}$ as a function of oxygen partial pressure. Temperature: (□) 1000 °C, (○) 800 °C and (△) 600 °C.

Table 1. Activation energies for Ba^{2+} and Mg^{2+} doped $LaGaO_3$

$La_{1-x}Ba_xGa_{1-y}Mg_yO_{3-\delta}$			High temperature activation energy/eV	Low temperature activation energy/eV
Notation	x	y		
LBGM-0020	0.00	0.20	0.58	1.23
LBGM-0025	0.00	0.25	0.60	1.23
LBGM-0510	0.05	0.10	0.56	1.17
LBGM-0515	0.05	0.15	0.59	1.08
LBGM-0520	0.05	0.20	0.62	1.09
LBGM-0525	0.05	0.25	0.63	1.11
LBGM-0530	0.05	0.30	0.67	1.16
LBGM-1000	0.10	0.00	0.52	0.67
LBGM-1005	0.10	0.05	0.59	0.73
LBGM-1010	0.10	0.10	0.57	0.94
LBGM-1015	0.10	0.15	0.59	0.98
LBGM-1020	0.10	0.20	0.62	1.03
LBGM-1025	0.10	0.25	0.58	1.08
LBGM-1030	0.10	0.30	0.63	1.12
LBGM-0020	0.00	0.20	0.58	1.23
LBGM-0520	0.05	0.20	0.62	1.09
LBGM-1020	0.10	0.20	0.62	1.03
LBGM-0025	0.00	0.25	0.60	1.23
LBGM-0525	0.05	0.25	0.63	1.11
LBGM-1025	0.10	0.25	0.57	1.08
LBGM-1525	0.15	0.25	0.62	1.06

3.3. *Activation energy*

The Arrhenius plot of log (σT) against $1/T$ should yield a straight line of slope $-E_a/k$ if activation energy E_a is independent of temperature in Equation 3. However, as shown in Figures 3, 4, 7 and 8, the Arrhenius plots are curved with different slopes in the high-temperature and low-temperature regions. This slope change has also been reported in LSGM system [9, 10, 12]. The activation energy (E_a) for oxygen ion conduction is usually the sum of a migration enthalpy (ΔH_m) and an association enthalpy (ΔH_a). In a low-temperature region, both are present due to association between dopant cations and oxygen vacancies, but in a high-temperature region, only a migration enthalpy (ΔH_m) is left since coulombic forces between dopant cations (negative defects) and oxygen vacancies (positive defects) decrease due to increased thermal energy. Therefore, the activation energy for oxygen ion conduction is much higher in a low-temperature region than in a high-temperature region.

The calculated activation energies are listed in Table 1. To exclude the effect of grain boundaries by second phases, the activation energies were calculated from σ_{bulk} data measured by a.c. impedance spectroscopy. The activation energies of oxygen migration in LBGM system were measured as 0.52–0.67 eV. These values are lower than those in LSGM system, 0.66–0.82 eV [9, 10, 12], but similar to those of $La_{0.90}Sr_{0.10}CoO_{3-\delta}$ (0.51 eV) and $La_{0.80}Sr_{0.20}CoO_{3-\delta}$ (0.59 eV) [13]. This difference may be due to the variation of the temperature range measured. As mentioned above, the activation energy in a high-temperature region can be taken as the migration enthalpy, ΔH_m for oxygen ion migration. The migration enthalpy has a tendency to increase slightly with increasing dopant concentration as shown in Table 1. This can be explained form the standpoint of the saddle point configuration of perovskite structure. The oxygen ions in perovskite structure move into adjacent oxygen vacancies along the $\langle 1\,1\,0\rangle$ edge of the BO_6 octahedron. In the saddle point configuration, the migrating oxygen ions must pass through the opening of a triangle with two A site cations and one B site cation. The energy barrier to pass through the saddle point is called the saddle point energy [14]. The lattice strain occurs by ion size mismatch due to the substitution of larger cation, Ba^{2+} (0.161 nm) or Mg^{2+} (0.072 nm), than host cation, La^{3+} (0.136 nm) or Ga^{3+} (0.062 nm), respectively. The saddle point energy increases with the resulting lattice strain. Consequently, the increased saddle point energy results in the increase in migration enthalpy.

Table 1 also shows that the activation energies of all compositions are much higher at low-temperature than at high-temperature. As mentioned above, this might be caused by the formation of $Mg'_{Ga} - V_{\ddot{O}}$ or $Ba'_{La} - V_{\ddot{O}}$ pair clusters at low-temperature. This also implies that the strong attractive interaction between Mg'_{Ga} and $V_{\ddot{O}}$ or between Ba'_{La} and $V_{\ddot{O}}$ causes the ionic conductivity to decrease at low-temperature. Moreover, the association enthalpy ($E_{a,\,low\ temp.} - E_{a,\,high\ temp.}$) of $LaGa_{0.80}Mg_{0.20}O_{3-\delta}$ (LBGM-0020) was 0.65 eV, while that of $La_{0.90}Ba_{0.10}GaO_{3-\delta}$ (LBGM-1000) was 0.15 eV. This

means that Mg^{2+} dopants have a much stronger tendency to be associated with the oxygen vacancies than the Ba^{2+} dopants at low-temperature. Khan et al. [15] reported that the binding energy of the $Mg'_{Ga} - V_{\ddot{O}}$ pair cluster is much higher than that of the $Sr'_{La} - V_{\ddot{O}}$ pair cluster because the ion size mismatch for Mg^{2+} on the Ga^{3+} sites is greater than the ion size mismatch for Sr^{2+} (0.144 nm) on the La^{3+} sites in the LSGM system. However, in this work, the activation energy in the low-temperature region decreased with increasing Ba^{2+} concentration despite the greater ion size mismatch for Ba^{2+} on the La^{3+} sites.

This different effect of Mg^{2+} and Ba^{2+} ion doping on the activation energy might be caused by the state of the cations in the perovskite structure rather than by ion size mismatch. In the perovskite structure, an oxygen ion is coordinated by six cations: with four A site cations and two B site cations. The length of the A–O fold is longer than that of the B–O fold. Therefore, the B–O fold has much stronger binding energy than the A–O fold. In other words, an oxygen vacancy might be more strongly associated with the Ga–O–Mg bond than the La–O–Ba bond in the Ba^{2+} and Mg^{2+} doped $LaGaO_3$ system. Consequently, the activation energy of Mg^{2+} doping is higher than that of Ba^{2+} doping. This is confirmed by the fact that, in spite of the same oxygen ion vacancy concentration, the oxygen ion conductivity value of $La_{0.90}Ba_{0.10}Ga_{0.70}Mg_{0.30}O_{3-\delta}$ (LBGM-1030) is much lower than that of $La_{0.85}Ba_{0.15}Ga_{0.75}Mg_{0.25}O_{3-\delta}$ (LBGM-1525) at low-temperature in Figure 8. Meanwhile, the reason for the increase in activation energy with increasing Ba^{2+} concentration in the low-temperature region is not yet clear. The reason is, however, probably related to the screening effect; large Ba^{2+} ions hinder the oxygen vacancies from associating with Mg^{2+} ions.

4. Conclusion

In the LBGM system, the increase in oxygen vacancies originating from the substitutions of cations with lower valence such as Ba^{2+} and Mg^{2+} is thought to make a contribution to the increase in oxygen ion conductivity. The oxygen ion conductivity value of $La_{0.90}Ba_{0.10}Ga_{0.80}Mg_{0.20}O_{3-\delta}$ (LBGM-1020) was 0.114 Ω^{-1} cm^{-1} at 800 °C, which is comparable to that of YSZ at 1000 °C. The grain boundary resistance decreased with increasing Mg^{2+} concentration due to a reduced second phase concentration, which was confirmed by microstructure observation. The activation energy of oxygen ion conduction was dependent on temperature and had a higher value in the low-temperature region. This may be caused by the formation of $Mg'_{Ga} - V_{\ddot{O}}$ or $Ba'_{La} - V_{\ddot{O}}$ pair clusters at low-temperature. Meanwhile, it is thought that Mg^{2+} have a much stronger tendency to be associated with oxygen vacancies than Ba^{2+} dopant. This can be explained by the state of the cations in the perovskite structure.

Thus, the LBGM system is a promising material as solid electrolyte for reduced-temperature ceramic fuel cells.

References

1. N.Q. Minh, *J. Am. Ceram. Soc.* **76** (1993) 563.
2. H. Yahiro, Y. Baba, K. Eguchi and H. Arai, *J. Appl. Electrochem.* **18** (1988) 527.
3. B.C.H. Steel, *Mater. Sci. Eng.* **B13** (1992) 79.
4. K.R. Kendall, C. Navas, J.K. Thomas and H.C. zur Loye, *Solid State Ionics* **82** (1995) 215.
5. T. Ishihara, H. Matsuda and Y. Takita, *J. Am. Chem. Soc.* **116** (1994) 3801.
6. K. Huang, M. Feng and J.B. Goodenough, *J. Am. Ceram. Soc.* **79** (1996) 1100.
7. P.N. Huang and A. Petric, *J. Electrochem. Soc.* **143** (1996) 1644.
8. T. Ishihara, M. Honda, T. Shibayama, H. Minami, H. Nishiguchi and Y. Tkita, *J. Electrochem. Soc.* **145** (1998) 3177.
9. J.W. Stevenson, T.R. Armstron, D.E. McCready, L.R. Pederson and W.J. Weber, *J. Electrochem. Soc.* **144** (1997) 3613.
10. K. Huang, R.S. Tichy and J.B. Goodenough, *J. Am. Ceram. Soc.* **81** (1998) 2565.
11. P. Kofstad, *in* E. Burke, B. Chalmers and James A. Krumhanst (Eds), 'Nonstoichiometry, Diffusion and Electrical Conductivity in Binary Metal Oxides' (Wiley-Interscience, New York, 1972), pp. 85–87.
12. J. Drennan, V. Zekuzko, D. Hay, F.T. Ciacchi, S. Rajendran and S.P.S. Badwal, *J. Mater. Chem.* **7** (1997) 79.
13. M.S. Islam, M. Cherry and C.R.A. Catlow, *J. Solid State Chem.* **124** (1996) 230.
14. J.A. Kilner and R.J. Brook, *Solid State Ionics* **6** (1982) 237.
15. M.S. Khan, M.S. Islam and D.R. Bates, *J. Phys. Chem. B* **102** (1998) 3099.
16. T. Ishihara, M. Honda, H. Nishicughi and Y. Takita, *Electrochem. Proc.* **97-18** (1997) 301.